Climatic Change
https://doi.org/10.1007/s10584-019-02524-4

Potential impacts of climate change on vegetation dynamics and ecosystem function in a mountain watershed on the Qinghai-Tibet Plateau

Decheng Zhou[1] · Lu Hao[1] · John B. Kim[2] · Peilong Liu[1] · Cen Pan[1] · Yongqiang Liu[3] · Ge Sun[4]

Received: 1 April 2019 / Accepted: 8 August 2019/Published online: 15 August 2019

Abstract
The Qinghai-Tibet Plateau constitutes unique mountain ecosystems that can be used for early detection of the impacts of climate change on ecosystem functions. We use the MAPSS-CENTURY 2 (MC2), a dynamic global vegetation model, to examine the potential responses of terrestrial ecosystems to climate change in the past (1961–2010) and future (2011–2080) under one medium-low warming scenario (RCP4.5) at a 1-km spatial resolution in the Upper Heihe River Basin (UHRB), northwestern China. Results showed that 21.4% of the watershed area has experienced changes in potential natural vegetation types in the past and that 42.6% of the land would undergo changes by the 2070s, characterized by a sharp increase in alpine tundra at the cost of cold barren land. Net primary productivity (NPP) and heterotrophic respiration (RH) have increased sharply since the mid-1980s and are projected to remain at reduced rates in the future. Overall, UHRB switched from carbon neutral to a carbon sink in 1961–2010, and the sink strength is projected to decline after 2040. Additionally, future climate change is projected to drive a decrease in water yield due to a slight decrease in precipitation and an increase in evapotranspiration (ET). Furthermore, we find large spatial variations in simulated ecosystem dynamics, including an upward trend of NPP, RH, and ET in the alpine zone, but a downward trend in the mid-elevation forest zone. These results underscore the complexity of potential impacts of climate change on mountain watersheds that represent the headwaters of inland river systems in an arid environment.

1 Introduction

Climate change, characterized by an increasing temperature and a suite of other alterations to the recent climate regime (e.g., greenhouse gases, precipitation, radiation), can strongly affect terrestrial

Electronic supplementary material The online version of this article (https://doi.org/10.1007/s10584-019-02524-4) contains supplementary material, which is available to authorized users.

✉ Lu Hao
haolu@nuist.edu.cn

Extended author information available on the last page of the article

ecosystems on timescales of decades to centuries (IPCC 2013). Mountains, covering approximately one-fourth of the global land area, constitute unique ecosystems for the early detection of climate change and for evaluation of the associated ecological responses (Beniston 2003). Climate in high elevations can change rapidly over a relatively short horizontal distance, resulting in a rich mosaic of ecosystems representing multiple latitudinal zones. Vegetation changes in high mountains are often more pronounced and easier to identify than those in lowlands owing to the high topographic and habitat gradients (Theurillat and Guisan 2001) and therefore are generally considered to be ecological indicators of climate change effects (Gobiet et al. 2014). At the same time, mountainous regions provide numerous ecosystem services to human society, including biodiversity, water resources, energy generation (hydropower), agricultural products, minerals, and recreation. Although only 26% of the global population resides in mountainous regions, over half of the global population depends on the ecosystem services provided by mountains (Beniston 2003). In particular, mountains are often recognized as "water towers" for the surrounding area, as mountains induce precipitation through orographic effects and then store water in their glaciers and snowpacks. This is particularly important in arid regions where precipitation is limited in lowlands and mountains are the primary source of water for downstream users.

The Heihe River Basin (HRB), located in arid northwestern China, is typical of many inland river basins in China. It houses over 1.46 million people and represents one of the most studied basins in China for understanding human-nature interactions (Cheng et al. 2014). Similar to other river basins in arid western China, the HRB has been increasingly experiencing water shortages due to rapid climate change and extensive anthropogenic disturbances, such as crop irrigation and urbanization, in recent years (Zhou et al. 2014). The Upper HRB (UHRB) is the area above 1700 m elevation, and it supplies approximately 70% of the total streamflow in the entire basin (Gao et al. 2016; Ruan et al. 2017). A systematic evaluation of possible future climate change impacts on the UHRB is crucial for formulating local climate change mitigation and adaptation strategies and for enhancing our understanding of the role of high elevation mountains in arid regions of the world.

The effects of climate change on ecosystems in the UHRB have been widely documented (Gao et al. 2016; Hao et al. 2016; Liu et al. 2017; Zhou et al. 2014). However, previous efforts have generally focused on a single-factor or short-term historical trends. For example, using a geomorphology-based hydrology model, Gao et al. (2016) concluded that the river runoff was mainly determined by the "cold barren" and alpine tundra land cover types. They simulated conditions between 1980 and 2010 and did not extend simulations into the future. Remote sensing studies documented an overall increasing trend of vegetation productivity in the UHRB from 1982 to 2012 due to a warming and wetting climate (Hao et al. 2016; Liu et al. 2017). To project vegetation dynamics under climate change scenarios and to predict how those changes will interact with the hydrology of the watershed, an integrated approach is needed, one that models the long-term climate-vegetation-water dynamics. Future projections for the UHRB are needed by regional policy-makers to manage various ecosystem services provided by the UHRB to the surrounding region.

Dynamic global vegetation models (DGVMs) have the ability to simulate interactions between climate, vegetation, and water under long-term climate change scenarios. They have been widely used to explore the effects of climate change on terrestrial ecosystems (Cramer et al. 2001). While there are many global applications of DGVMs (Gonzalez et al. 2010; Kim et al. 2017), those results do not have sufficient spatial resolution or satisfactory calibration for a focused regional-scale analysis. DGVMs have been calibrated for specific regions using region-specific datasets (Case et al. 2018; Kim et al. 2018). The limited availability of fine

resolution climate data and other ancillary datasets at the regional scale is a significant challenge to regional applications of DGVMs. Although climate change projections from general circulation models are widely available, they are generally too coarse and often fail to adequately capture the local climate. For example, they fail to capture precipitation patterns in a mountainous region with a complex terrain (Beniston 2003). Some downscaled climate projections are available but are generally limited to North America and Europe (Palomo 2017). In addition, the soil data required for modeling vegetation dynamics have poor spatial accuracy for many mountainous regions of the globe.

In this study, we explored the responses of vegetation and ecosystem functions to historical (1961–2010) and projected future (2011–2080) climate changes at a 1-km spatial resolution in the UHRB. We used MAPSS-CENTURY 2 (MC2) DGVM (Bachelet et al. 2001; Conklin et al. 2016), which simulates vegetation biogeography, biogeochemistry, and interactions with fire on a gridded landscape. Our objectives were to (1) calibrate and evaluate MC2 to the UHRB using the best available data and (2) characterize the simulated impacts of climate change on the potential vegetation type and two key ecosystem services: carbon sequestration and the water budget. This study represents the first modeling effort in this high population region where vegetation dynamics are modeled across a large scale over a long-term. In addition, it is the first regional application of MC2 outside of North America, the continent in which the model was originally developed.

2 Methods

2.1 Study area

The Heihe River Basin (HRB) is a 128,900 km^2 watershed in northwest China (Fig. 1a). The Upper HRB (UHRB) (98° 34′–101° 11′ E, 37° 41′–39° 05′ N), with a total area of 10,005 km^2, is located along the southern edge of the HRB (Fig. 1b). With elevations ranging from 1700 to 2500 m, the UHRB is a part of the Qinghai-Tibet Plateau. The UHRB has climate, vegetation, and socioeconomic conditions distinct from the rest of the HRB (Cheng et al. 2014). Climate varies substantially across the complex topography of the UHRB, with a mean annual precipitation ranging from 161 to 721 mm and a mean annual temperature ranging from − 9.9 to 6.4 °C (Fig. A1). The complex mosaic of vegetation can be classified into major vegetation types for modeling and analysis including cold barren (Saussurea DC., Cremanthodium DC., and *Rhodiola rosea* L.), alpine tundra (Kobresia parva, Kobresia humilis, and Kobresia tibetica), shrub (Potentillafruticosa Linn, *Dasiphora fruticosa*, Caragana jubata, and Salix gilashanica), forest (Piceacrassifolia Kom), grass (*Abietinella abietina*, Stipapurpurea Griseb, Stipa purpurea, Stipa przewalskii, and Carex kansuensis), and desert (Symplegma regelii Bunge). The soils in the UHRB are dominated by alpine frost (silty-sand textured), felty (silty-sand textured), and chestnut (sandy textured) soils (Qin et al. 2016b). The soils are generally deeper than 20 cm (Fig. A1) with a mean depth of 71 cm. Soil organic carbon (SOC) exceeds 15 g kg^{-1} (Song et al. 2016), with more SOC in the permafrost layer than in the active layer (Mu et al. 2014).

2.2 MC2 dynamic global vegetation model

MC2 is a computationally efficient version of the MC1 DGVM designed to simulate the effects of climate change and wildfires on vegetation together with ecosystem structure

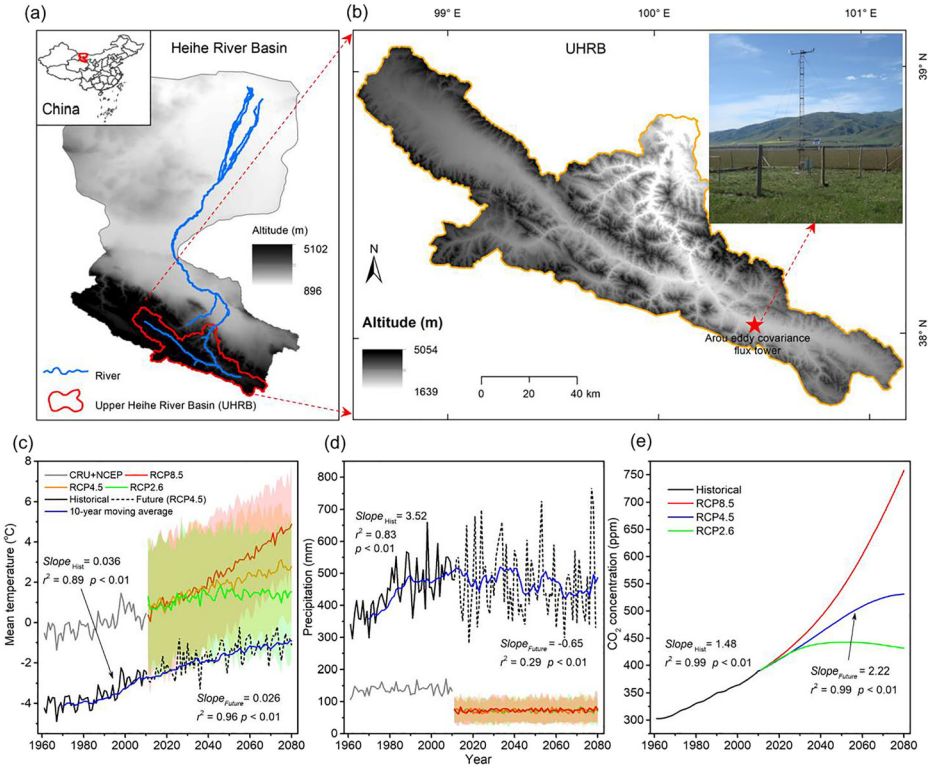

Fig. 1 Location of the Upper Heihe River Basin (UHRB) (**a**, **b**) and the historical (1961–2010) and projected future (2011–2080) mean annual temperature (**c**), total precipitation (**d**), and CO_2 concentrations (**e**). Historical climate data (CRU+NCEP) (Wei et al. 2014) used in the Multiscale Synthesis and Terrestrial Model Intercomparison Project (MsTMIP) (Shim et al. 2014) and climate projections from five global climate models (BNU-ESM, IPSL-CM5A-MR, MPI-ESM-LR, MPI-ESM-MR, NorESM1-M) published by the Coupled Model Intercomparison Project Phase 5 (CMIP5) covering the UHRB are also shown in panels **c** and **d**. The shaded area represents one standard deviation computed from the five climate models

and function. MC1 and MC2 have been used in regional, continental, and global studies (Bachelet et al. 2015; Bachelet et al. 2003; Sheehan et al. 2015). Details of MC2 design are documented elsewhere (Bachelet et al. 2001; Conklin et al. 2016). Here, we summarize the salient features of MC2. MC2 comprises three linked modules: the MAPSS biogeography model (Neilson 1995); a modified version of the CENTURY Soil Organic Model (Parton et al. 1993) for simulating biogeochemistry; and MC-FIRE (Lenihan et al. 1998), which simulates fire occurrence and its effects. MC2 runs on a monthly time step and represents the landscape as a grid with no interaction among grid cells. In each grid cell, the model simulates the competition for light, water, and nutrients between trees and grass. Every month, the biogeochemistry module calculates the water budget for each grid cell and calculates vegetation productivity and the carbon budget. Productivity is constrained by temperature and soil moisture according to vegetation type-specific parameters. The fire module converts carbon stocks into fuel models according to species-specific parameters. Fire occurrence is determined using thresholds on two fuel moisture indices. Annually, the biogeography module classifies each grid cell into a vegetation type.

MC2 is run in four successive phases. In the first phase, the model uses the 1961–1990 climatology to predict potential vegetation biogeography and to spin up the soil carbon pools until they stabilize. In the second phase, the model is run for 2000 years with detrended historical climate until a dynamic equilibrium among vegetation, wildfire, and climate is reached. The detrended historical climate data were created from the period 1961–1990 following Drapek et al. (2015), where the climate values are converted to anomalies relative to a 30-year moving window average and then added to the 1961–1975 climatology. The third and fourth phases are the simulations of historical and future conditions, where the model is run using transient climate data to simulate the response of vegetation to historic and projected future climate.

2.3 Input data

We obtained 1-km spatial resolution monthly climate data (minimum temperature, maximum temperature, precipitation, and vapor pressure) for the UHRB from 1961 to 2012 from Wang et al. (2016) and Ruan et al. (2017). These were climate reanalysis data based on 15 national meteorological stations, 25 hydrological stations, and the RIEMS 2.0 regional climate model (Xiong and Yan 2013). Since Wang et al. (2016) and Ruan et al. (2017) described the datasets in detail, here, we summarize only the salient characteristics of the dataset. RIEMS 2.0 accurately captures the seasonal and spatial patterns of the climate in the UHRB, although it may overestimate precipitation (Xiong and Yan 2013). The weather and hydrological stations provide accurate local climate data. This reanalysis data is superior to global datasets, with R^2 between the interpolated and observation values larger than 0.7 at the monthly scale (Wang et al. 2016). The mean annual temperature and precipitation in the UHRB are substantially overestimated and underestimated by the global-scale climate data, respectively (Fig. 1c, d) (Wei et al. 2014), suggesting possible underestimation of the ecosystem productivity and evapotranspiration in the UHRB by global-scale simulations.

We also obtained one future climate projection available from RIEMS 2.0. The climate projection is based on RCP4.5, the medium-low warming scenario from the IPCC Fifth Assessment Report (AR5), and spans 2006 to 2080 (Xiong and Yan 2013). The 3-km resolution output from RIEMS 2.0 was downscaled to 1 km using the delta method (Drapek et al. 2015). First, the data from RIEMS 2.0 were resampled to a spatial resolution of 1-km using bilinear interpolation method to represent the climate change trends of all grids. Second, the difference (precipitation and vapor pressure) or ratio (temperature) of climate reanalysis data to RIEMS data, reflecting the corrected climate and the spatial variability, was calculated based on the data in the overlapped time period of 2006–2012 for each month and each individual grid. Finally, we added the differences or multiplied the ratios to the modeled data over the period of 2011–2080 by assuming the same spatial variability of climate through the time. The resultant data project the mean annual temperature to increase continuously from 2011 to 2080 at an annual rate of 0.026 °C, while precipitation is projected to decrease slightly during the same period (Fig. 1d). The annual mean temperature and total precipitation were significantly lower and higher, respectively, than values estimated by global circulation models (GCMs) data published by the Coupled Model Intercomparison Project Phase 5 (CMIP5), respectively (Fig. 1c, d).

We obtained 90 m soil data from Song et al. (2016) and Yang et al. (2016), which were generated by soil-landscape models based on 548 sampling points within the HRB (Fig. A1). We extracted the 90-m elevation data from ASTER GDEM version 2 (Tachikawa et al. 2011).

The soil and elevation data were resampled to 1 km to align with the climate data. For atmospheric CO_2 concentrations under RCP 4.5, we used values published by Meinshausen et al. (2011), where they increase continuously from 2006 to 2080 at a rate of 2.22 ppm $year^{-1}$ (Fig. 1e).

2.4 Model calibration

We used a structured approach to calibrate MC2 (Table 1), following an application of MC2 to a mountainous region in the USA (Kim et al. 2018). First, we calibrated the model for net primary production (NPP) and maximum leaf area index (LAI) with the fire module disabled. We adjusted the water- and temperature-based productivity coefficients and the potential aboveground monthly production limits to obtain model output that matched the Moderate Resolution Imaging Spectroradiometer (MODIS) gridded NPP estimates (MOD17A3) (Running and Zhao 2015). We adjusted the maximum LAI limits so that the simulated LAI matched the GLASS LAI version 3.0 (Xiao et al. 2016). MODIS and GLASS data exhibit good performances in mountainous areas (Jin et al. 2017; Shim et al. 2014).

In the second stage of calibration, we adjusted the MC2's biogeography rules so that the model output matched an actual vegetation map for the UHRB (Zhang et al. 2016). Vegetation cover types in the UHRB are primarily controlled by natural factors (Cheng et al. 2014). We adjusted the temperature thresholds for the climate zones and carbon and productivity thresholds for the biomes and vegetation types. We grouped the actual vegetation types into the six vegetation types defined by MC2: cold barren (with no or very sparse vegetation and boreal climate), alpine tundra, forest (boreal evergreen needleleaf forest), shrub/grass (boreal shrubland, temperate shrubland, temperate grassland), and desert (with sparse vegetation and temperate climate). We did not separate grassland from shrubland because of its small area percentage and the high probability of it being misclassified as shrubland in MC2. The primary difference between cold barren and desert was the climate zone. As the final step, we turned on the fire module and repeated the calibration stages described above.

2.5 Model evaluation

Model output was evaluated against multiple benchmark datasets. First, we compared simulated net ecosystem production (NEP) and evapotranspiration (ET) at an alpine tundra site against in situ observations (2008–2011) at the Arou eddy covariance flux measurement tower site (Fig. 1b). The data were provided by the Cold and Arid Regions Science Data Center (Liu et al. 2018). The simulated monthly NEP and ET values had excellent correspondence with the measured values, with R^2 values of 77% and 84% and RMSE values of − 12.5 g C m^{-2} and − 2.6 mm for NEP and ET, respectively (Fig. 2a, b).

At the regional scale, the model output had moderately successful agreement with benchmark datasets. Simulated NPP over forestlands agreed well with the MODIS NPP in terms of interannual variability ($r = 0.86$, $p < 0.01$) (Fig. 2c). The simulated total NPP (364.4 ± 29.9 g C m^{-2} $year^{-1}$, mean ± one standard deviation hereafter) was clearly larger than the MODIS NPP (272.5 ± 18.0 g C m^{-2} $year^{-1}$) during 2000–2012, although NPP by tree (208.2 ± 29.9 g C m^{-2} $year^{-1}$) was lower. A similar phenomenon was observed in the maximum LAI when compared to the GLASS LAI products, where the model overestimates total LAI (Fig. 2d). We also compared the simulated ET with the 1 km estimates produced by ETWatch (Wu et al. 2016). ETWatch is based on multi-source remotely sensed data and has been

Table 1 MC2 parameters calibrated for the study

Parameter	Description	Default	Calibrated
bz_thres (°C)	Upper limit of low monthly temperature for the boreal climate zone	−15	−17
t_low (°C)	Upper limit of low monthly temperature for needleleaf tree type	−15	−25
t_mid (°C)	Lower limit of low monthly temperature for broadleaf tree type	1.5	−13.5
p_low (mm)	Upper limit of warm season precipitation for evergreen tree type	70	56
p_hi (mm)	Lower limit of warm season precipitation for deciduous tree type	90	105
pprdwc (a, b, c) (dimensionless)	Productivity coefficient that represents how much water is available to the trees	(0.5, 1, 0.9)	(0.3, 1, 0.6)
ppdf(1) _EN (°C)	Optimum (ppdf(1)) and maximum (ppdf(2)) temperatures for production for	15	20
ppdf(1) _DB (°C)	parameterization of a Poisson density function curve to simulate temperature	22	23
ppdf(1) _C3 grass (°C)	effect on growth for evergreen needleleaf (EN) tree type, deciduous broadleaf	18	12
ppdf(2) _EN (°C)	(DB) tree type, and C3 grass.	30	30
ppdf(2) _DB (°C)		35	41
ppdf(2) _C3 grass (°C)		32	22
max_NPP_EN/DB (g C m^{-2})	Potential aboveground monthly production for EN and DB	250	250
max_NPP_C3 grass (g C m^{-2})	Potential aboveground monthly production for C3 grass	150	120
max_LAI (m^2 m^{-2})	Maximum leaf area index for EN and DB	8	4
forest_thres (g C m^{-2})	Lower limit of total tree carbon for forest	3000	2500
woodl_thres (g C m^{-2})	Upper limit of tree carbon for shrubs	1150	800
desert_treec_max (g C m^{-2})	Upper limit of tree carbon for deserts	27	300
desert_grassc_max (g C m^{-2})	Upper limit of grass carbon for deserts	385	150
grassfrac_thres	Lower limit of grass fraction for grassland	0.6	0.5

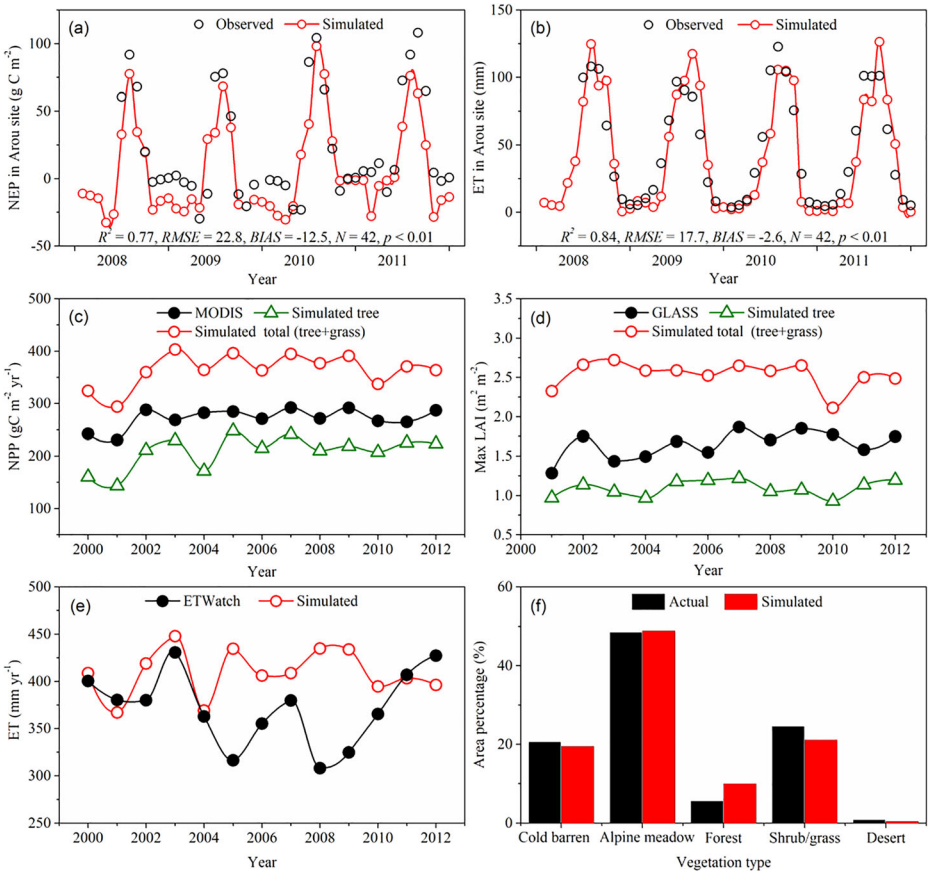

Fig. 2 Comparisons of the simulated net ecosystem production (NEP) (**a**) and evapotranspiration (ET) (**b**) with in situ observations at the Arou eddy covariance flux tower site, simulated watershed mean annual net primary production (NPP) (**c**), leaf area index (LAI) (**d**), and ET (**e**) with remotely sensed estimates over forests, and the simulated potential vegetation with observed actual vegetation (**f**) in the Upper Heihe River Basin. Since simulated LAI and NPP for each grid cell are composed of two parts, tree and grass, we compare the remotely sensed estimates with the simulated total (tree + grass) and the tree portion separately

demonstrated to accurately estimate ET for semiarid regions with an accuracy greater than 90.7% (Wu et al. 2016). The ET estimated by MC2 was slightly higher than that estimated by ETWatch (Fig. 2e). These overestimates are reasonable since grazing effects are not simulated by MC2 and grazing may reduce NPP, LAI, and ET contributions by grass (Liu et al. 2017). Additionally, the simulated streamflow (~210 mm year^{-1}) was comparable to the previous estimates (~185 mm^{-1}) (Yang et al. 2015; Yang et al. 2017) over the entire UHRB during the 2001–2010 period.

The model captured the broad spatial patterns of vegetation distribution—particularly the cold barren and alpine tundra—with a general agreement of 59% during 2001–2010 (Figs. 2f and A2). There were high disagreements in some areas dominated by forest and shrub/grass. In particular, the simulated potential forestland area was 1.77 times the actual forest area (Fig. 2f). The disparity might be attributed to the difference between potential and actual natural vegetation and the data limitations that will be discussed later. For example, long-term human activities such as farmland reclamation and grazing may have affected vegetation distribution

in the study area (Cheng et al. 2014), a mechanism not simulated in our study. The 1-km spatial resolution of the climate data may also contribute to the error in biogeography, as many topographic features and associated climate factors at finer scales may help determine vegetation biogeography (Fig. A1) (Qin et al. 2016b).

3 Results

Ecosystem characteristics simulated by MC2 exhibited distinct trends from 1960 to 2080 under the RCP4.5 climate change scenario. Below, we characterize those trends as well as contrast projected future (2051–2080) ecosystem characteristics vs. historic (1961–1990) characteristics. Fire effects simulated by MC2 were negligible, with an annual mean carbon loss of only 0.06 g C m^{-2} due to fire (Fig. A3).

3.1 Changes in potential vegetation distribution

Climate change is projected to substantially alter vegetation distribution in the UHRB (Fig. 3). The UHRB was dominated by alpine tundra and cold barren vegetation types in the 1960s, occupying 35.3% and 35.7% of the total area, respectively (Fig. 3a). One of the most striking patterns of vegetation shifts is the conversion of the cold barren type to alpine tundra (Fig. 3d–e). Concurrently, the conversions from alpine tundra to shrub/grassland and from shrub/grassland to forest were also significant. For example, approximately 11.2% and 55.9% of the shrub/grasslands in the 2000s and the 2070s were alpine tundra in the 1960s. In our simulation, approximately 12.2% of the shrub/grasslands in the 1960s were transformed into forests by the 2000s and 35.5% of the shrub/grassland in the 2000s shifted into forests by the 2070s. Overall, approximately 21.4% of the study area has been simulated to have shifted in potential vegetation type during the past 50 years (Fig. 3d), and 42.6% of the land area was projected to undergo a change by the 2070s compared to the 2000s (Fig. 3e).

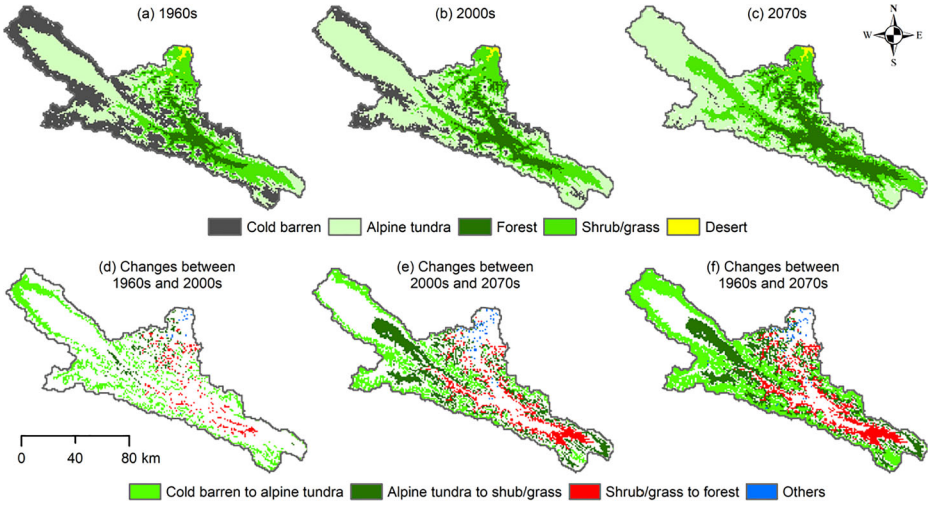

Fig. 3 Spatial distributions of the simulated potential vegetation over the 1960s (**a**), 2000s (**b**), and 2070s (**c**), and the vegetation shifts between time periods (**d**, **e**, **f**) in the Upper Heihe River Basin

Inter-decadal changes of area percentages of different vegetation types are presented in Supplementary Material Fig. A4. Alpine tundra showed little change prior to the 1980s and then increased dramatically to 55.4% in the 2020s, followed by a small decrease. Cold barren land decreased continuously and sharply after the 1980s to only 2.5% in the 2070s. Comparatively, the shrub/grassland remained nearly constant at approximately 21% in the past 50 years and is projected to increase gradually to 30.8% by the 2070s. Forests expanded consistently from 7.4% in the 1980s to 17.3% in the 2070s. Desert, occupying less than 1% of the total land area, showed little change during the entire study period.

Projected shifts in vegetation types are associated with changes in productivity, as reflected in the maximum LAI. Before the mid-1980s, the maximum LAI averaged across the region remained stable but is projected to exhibit a sharp increase thereafter (Fig. 4a). LAI trends varied greatly across space. It increased in high elevation areas dominated by cold barren and alpine tundra and low mountains dominated by desert and shrub/grass, but decreased in mid-mountain areas dominated by shrub/grass and forest (Fig. 5a, b). On average, a 44% increase of maximum LAI (2.48 vs. 1.72 m^2 m^{-2}) was projected in the future (represented by the mean estimate in 2051–2080) relative to historical conditions (1961–1990).

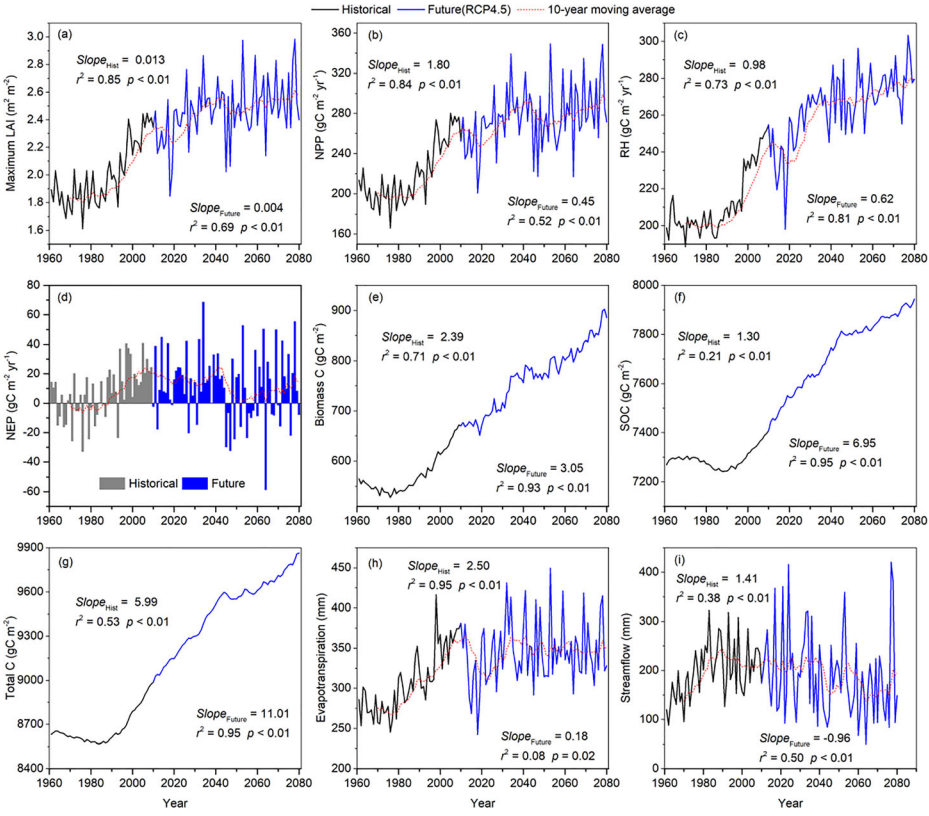

Fig. 4 Simulated maximum LAI (**a**), net primary productivity (NPP) (**b**), heterotrophic respiration (RH) (**c**), net ecosystem productivity (NEP) (**d**), total vegetation carbon (**e**), soil organic carbon (SOC) (**f**), total ecosystem carbon (**g**), evapotranspiration (**h**), and streamflow (**i**), for the Upper Heihe River Basin. Future simulation is based on RCP4.5 climate change scenario. Slope, the coefficient of determination (r^2) and significance (p) shown are calculated from linear regression separately for values in the historical period (1961–2010) and for values in the future (2011–2080)

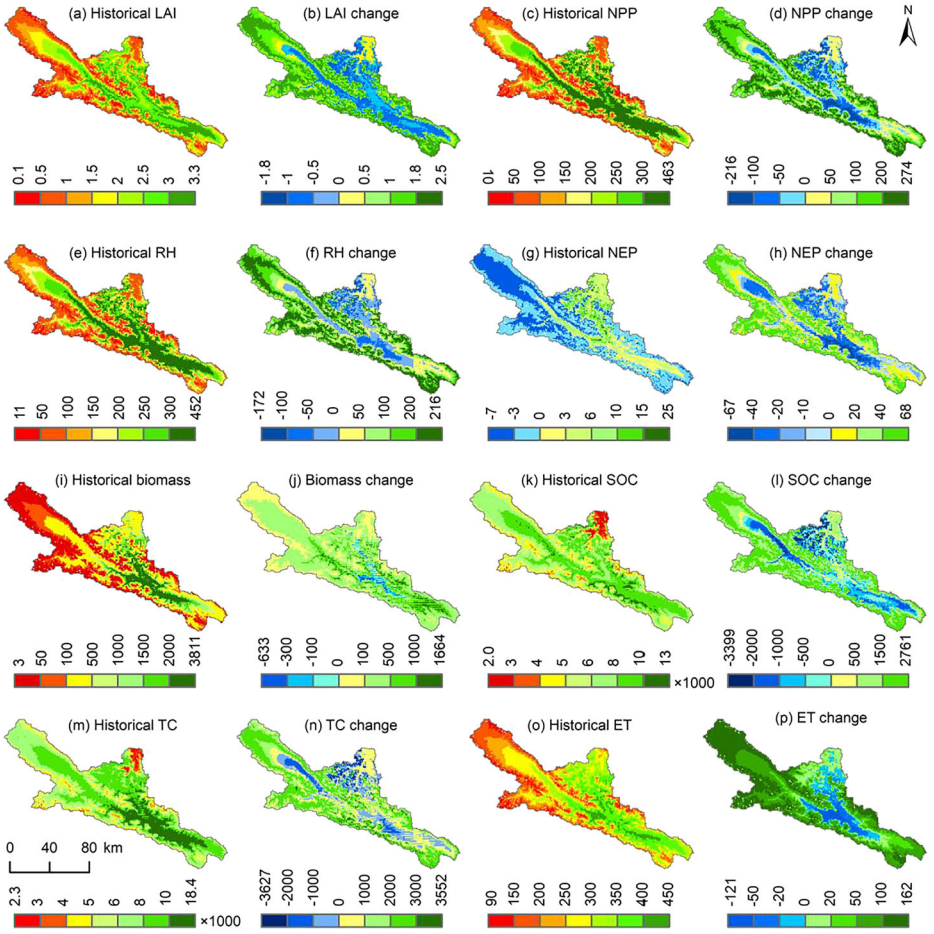

Fig. 5 Maps of historical (1961–1990) averages of key ecosystem variables and their projected changes in the future (2051–2080). The ecosystem variables are maximum leaf area index (LAI) (**a**, **b**); net primary productivity (NPP) (**c**, **d**); heterotrophic respiration (RH) (**e**, **f**); net ecosystem productivity (NEP) (**g**, **h**); total vegetation carbon (biomass) (**i**, **j**); soil organic carbon (SOC) (**k**, **l**); total ecosystem carbon (TC) (**m**, **n**); and evapotranspiration (ET) (**o**, **p**)

3.2 Changes in carbon budgets

Climate change exerted a strong effect on the simulated carbon dynamics of the study area. The area-weighted mean NPP increased significantly from the mid-1980s, with an annual increase rate of 1.80 g C m^{-2} $year^{-1}$ from 1961 to 2010 (Fig. 4b). In the future, the NPP was projected to increase at a much lower rate at 0.45 g C m^{-2} $year^{-1}$. Heterotrophic respiration (RH) exhibited a similar trend (Fig. 4c), but its annual growth rate was clearly lower than that of the NPP in the past and slightly higher than the NPP in the future. Consequently, the UHRB switched from being nearly carbon neutral (NEP < 5 g C m^{-2} $year^{-1}$) to becoming a carbon sink (positive NEP) during 1961–2010. The carbon sink strength was simulated to reach a maximum of approximately 20 g C m^{-2} $year^{-1}$ in 2040 and then decrease gradually afterwards (Fig. 4d). The cumulative carbon sequestration was projected to reach 1.2 kg C m^{-2} by 2080. Ecosystem carbon pools, including biomass, SOC, and total ecosystem carbon, decreased

slightly prior to the mid-1980s and was then projected to increase consistently by the end of the study period (Fig. 4e–g). In general, the rate of increase was projected to be higher in the future than in the past, especially for SOC. For example, the rate of increase of SOC was 7.0 g C m^{-2} $year^{-1}$ in the future, 5.3 times the rate estimated for 1961–2010.

There were large spatial variability in carbon fluxes, carbon pools, and their long-term trends (Fig. 5c–n). The mid-elevations covered mainly by shrub/grass and forests had the largest NPP and RH (Fig. 5c, e). The combined effect was that the mid-mountains generally functioned as a weak carbon sink (less than 25 g C m^{-2} $year^{-1}$) in the past (Figs. 5g and A5). Low elevations, covered mainly by desert and shrub/grass, also acted as weak carbon sinks although with relatively lower NPP. In contrast, cold barren and alpine tundra lands behaved as carbon sources in 1961–1990 (Fig. A5).

Spatial variability of carbon fluxes extended into future projections, as evidenced by increasing fluxes in the high mountains and decreases in the mid-mountains (Fig. 5d, f, h). On average, NPP and RH increased by 84.9 and 74.7 g C m^{-2} $year^{-1}$ in 2051–2080 relative to the rates in 1961–1990, respectively, leading to a net increase in NEP of 10.1 g C m^{-2} $year^{-1}$. In particular, forest is projected to become a significant carbon source by 2051–2080, while the cold barren type is projected to become a carbon sink (Figs. 5h and A5). Overall, carbon stocks showed similar spatial patterns to carbon fluxes (Fig. 5i–n). For example, vegetation biomass, accounting for 6.4% of the total carbon, was projected to increase by 50.8% (a net increase of 278.2 g C m^{-2}) in the future compared to the baseline (Fig. 5j). Concurrently, SOC is projected to be enhanced by 12.5% in the future, with a net growth of 1073.3 g C m^{-2} (Fig. 5l).

3.3 Changes in water budgets

MC2 simulated large increases in ET in the past 50 years, except for a slight decrease prior to the 1980s (Fig. 4h). However, ET was projected to increase slightly (0.18 mm $year^{-1}$) in the future period, albeit with large fluctuations. Spatially, the mid-mountains had relatively higher ET due to higher precipitation and vegetation productivity (Fig. 5o, p). ET is projected to increase in the high mountains and decrease in some of the middle mountainous areas in the future (Fig. 5p) under the RCP4.5 scenario. Modeled streamflow decreased slowly since the mid-1980s after a period of rapid increase. Streamflow is projected to decrease continuously in the future at a rate of 0.96 mm $year^{-1}$ (Fig. 4i). Overall, ET is projected to increase by 21.8% (287 to 349 mm) in 2051–2080 relative to 1961–1990. Streamflow is projected to decrease by 8.4% (191 to 175 mm) in the future.

4 Discussion

4.1 Impacts of climate change on vegetation distribution

Climate change is expected to bring significant changes to the structure and function of ecosystems in the UHRB (Fig. 1b). The temperature increase rate of 0.36 °C per decade from 1961 to 2010 was twice of the global average (IPCC 2013) and much higher than the average for China (Qin et al. 2016a). This is highly consistent with observations that higher rates of warming are often found in high latitudinal and altitudinal regions (Gobiet et al. 2014). At the same time, increasing precipitation in the UHRB agrees well with the overall wetting trend observed in arid/semiarid China (Qin et al. 2016a). Together, these two facets of climate

change have favored vegetation growth in the UHRB from 1961 to 2010. However, slightly decreasing precipitation and continuous warming in temperature were projected in the future (Fig. 1b), which may reduce water availability and create drought conditions that threaten many of the vegetated ecosystems.

Climate change is projected to drive a considerable amount of vegetation shifts in the UHRB. The most significant change is a sharp increase in alpine tundra at the cost of the cold barren vegetation type and a moderate growth of forest and shrub/grass lands (Fig. 3). Overall, this is in line with remotely sensed observations in the study area. For example, Yang et al. (2017) found a clear increase in pasture and forestland, with a decrease in barren land and glacier in the 1980s and 2000s. Zhao et al. (2017) showed that the grassland area (alpine tundra + grassland) increased by 19.7% from 1986 to 2011. The loss of the cold barren vegetation type is also partially corroborated by the significant increase of leaf area index in the high elevation regions in the UHRB (Liu et al. 2017).

Our findings were highly consistent with the previous findings on mountainous vegetation shifts in response to climate change (Gottfried et al. 2012; Hickler et al. 2012). Theoretically, vegetation distributions are mainly determined by climate regimes through species-specific physiological thresholds of temperature and/or water availability (Woodward 1987). Warming temperatures favor the growth of warm-adapted species, the process of which is commonly referred to thermophilization (Gottfried et al. 2012). In particular, the cold barren land would almost disappear by 2080. Such a potential vegetation shift has already been observed in other mountain regions such as the Alps (Gottfried et al. 2012). Overall, we project a change of vegetation of 42.6% of the total study area by the 2070s, which is comparable to projections in Europe (Hickler et al. 2012; Theurillat and Guisan 2001). For example, Hickler et al. (2012) indicated that over 42% of the land in Europe would undergo a change in vegetation by the 2080s in the arctic and alpine regions.

4.2 Impacts of climate change on vegetation structure and ecosystem functions

Vegetation structure, as represented by maximum LAI, was strongly influenced by climate change, with dominant drivers varying over time. In the historical period, the simulated LAI was overwhelmingly controlled by temperature, with a partial correlation coefficient (r) of 0.82 ($p < 0.01$) and an independent explanation rate of 74.5% (Table 2). These findings agree well with the well-established concept that temperature mainly controls vegetation dynamics in the high elevation regions (You et al. 2018; Zhou et al. 2014). In contrast, precipitation ($r = 0.64$, $p < 0.01$) is projected to play a more important role than temperature ($r = 0.48$, $p < 0.01$) in the future. This can be attributed to the increasing water stress caused by warming temperatures and decreasing precipitation (Fig. 1b). In addition, there is a great deal of spatial heterogeneity in the LAI trends (Fig. 5b). The mid-mountains exhibit a downward trend, possibly owing to the stronger control of water availability on vegetation growth as compared to temperature (Liu et al. 2017). The deceasing precipitation projected for the UHRB (Fig. 1b) reduces the water availability for plant growth in those areas.

Carbon fluxes and sequestration potential are projected to change dramatically in the future (Fig. 4b–i). The area-weighted mean NPP is simulated to have increased significantly in the past (Fig. 4b), driven primarily by temperature increase (Table 2). Because temperatures are generally lower than the optimal temperatures for plant growth in the UHRB (You et al. 2018), warmer temperatures can enhance productivity and biomass formation by lengthening the growing season and promoting photosynthesis where ample moisture is available (Nemani et al. 2003). At the same

Table 2 Partial correlation coefficients (r) between annual mean temperature (T) and ecosystem variables while holding annual precipitation (P) as the control variable, and between P and ecosystem variables while holding T as the control variable during historical (1961–2010) and future (2011–2080) time periods. The independent explanation rate (R^2, %) of P and T was derived from stepwise multiple linear regression analysis

Ecosystem variables	Correlation	Historical ($N = 50$)			Future ($N = 70$)		
		T	P	Total	T	P	Total
Maximum leaf area index	r	0.82+	0.24		0.48+	0.64+	
	R^2	74.9+	1.4	76.3	15.9+	31.3+	47.2
Net primary production	r	0.81+	0.12		0.43+	0.60+	
	R^2	72.6+	0.4	73.0	13.0+	28.6+	41.6
Heterotrophic respiration	r	0.78+	0.29*		0.65+	0.51+	
	R^2	70.6+	2.5*	73.0	31.6+	17.9+	49.5
Net ecosystem production	r	0.55+	−0.07		−0.02	0.42+	
	R^2	33.9+	0.3	34.2		18.2+	18.2
Evapotranspiration	r	0.78+	0.64+		0.42+	0.78+	
	R^2	68.4+	13.0+	81.5	8.0+	54.0+	62.0
Streamflow	r	−0.75+	0.96+		−0.23	0.96+	
	R^2	9.5+	83.0+	92.5	0.4	91.7+	91.9

+ Significant at the 0.01 level

*Significant at the 0.05 level

time, elevated CO_2 can influence NPP with the "CO_2 fertilization effect" (Cramer et al. 2001), where photosynthetic rates increase and water loss is reduced via closure of the stomata. However, soil water losses associated with rising temperatures may largely dwarf the positive effects of temperature. This may explain the much lower rates of increase in NPP in the future when precipitation tends to decrease (Fig. 4b). In fact, future NPP variability was found to be mainly controlled by precipitation though temperature also matters (Table 2). The concurrent increase in RH (Fig. 4c) is consistent with the acceleration of biospheric metabolism reported by Luo et al. (2001). The link between temperatures and RH is verified by the significant positive relationship between the two (Table 2). NEP, representing the carbon sequestration potential, fluctuated substantially year-by-year and generally increased in the historic period (Fig. 4d). The carbon sink strength in the UHRB is projected to reach its upper limit by approximately 2040, agreeing well with the findings by Tao and Zhang (2010) in China. Overall, we estimated a net carbon sink of 7.3 g C m^{-2} $year^{-1}$ in the UHRB over the past 50 years, which was much lower than the area-weighted mean estimate in China (23.3–31.9 g C m^{-2} $year^{-1}$) (Piao et al. 2009), suggesting a weak contribution of arid mountainous ecosystems to global carbon sequestration.

Simulated carbon budgets vary spatially and temporally in the UHRB. Mid-mountains that have the most favorable water and heat conditions exhibited larger NPP, RH, and NEP values than other areas at either high or low elevations (Fig. 5c–n). With the warming and drying climate in the future, carbon fluxes will be largely enhanced in the high mountains and reduced in the mid-mountains owing to the possible contrasting driving mechanisms. High mountains are overwhelmingly controlled by temperature. Elevated temperatures can increase the vegetation productivity and greening when moisture is not limiting (Nemani et al. 2003). In particular, lands covered by the cold barren vegetation type previously are projected to become the largest carbon sink across the UHRB in the future (Fig. A3). Comparatively, the mid-elevations are dominated by both temperature and water availability. Increasing temperature and/or decreasing precipitation would exacerbate the water shortages, therefore reducing the vegetation productivity. This would result in ecosystems switching from carbon sinks to carbon sources in the future (Fig. A5).

Simulated water balance also exhibited strong future trends because water and carbon are intrinsically coupled. The simulated ET, on average accounting for 73% of the total precipitation, increased significantly from the mid-1980s due to climate change-induced increases in vegetation productivity and potential evapotranspiration (Zhou et al. 2014). It was projected to increase at a rather low rate in the future, most likely owing to the small decrease in precipitation (Fig. 1b) and slow increase in LAI (Fig. 4a). As with NPP, the interannual variability of ET is mainly controlled by temperature in the past and by precipitation in the future (Table 2). Spatially, higher ET has been observed in the mid-mountains, echoing the fact that forest contributed little to the water yield in the UHRB (Ruan et al. 2017; Zhang et al. 2015). In contrast, the alpine tundra and cold barren lands contributed mainly to the water yield in the UHRB, which was highly consistent with previous findings (Yang et al. 2015; Ruan et al. 2017). Modeled streamflow decreased continuously since the mid-1980s and the trend will continue in the future due to the decrease in precipitation and the increase in ET, suggesting the possible exacerbation of water shortages in the entire river basin in the future. In contrast to ET, changes in streamflow were mainly determined by precipitation regardless of the time period (Table 2). Note that declines are seen in simulated LAI, NPP, RH, and ET from 2010 to 2020 (Fig. 4). This is likely an artifact of the model transitioning from the historical to future climate data.

4.3 Implications and uncertainties

This study presents a comprehensive, long-term assessment of the vegetation distribution and ecosystem dynamics in response to climate changes in the UHRB. This type of exploration is key for formulating the effective management strategies of local ecosystems (Zhou et al. 2014). Significant changes are projected in potential vegetation types, vegetation structure, and ecosystem functions in the UHRB, which may seriously impact the provision of ecosystem services and may therefore impact the livelihoods of local residents. In particular, the projected decrease in streamflow in the UHRB will exacerbate water shortages in the middle-lower reaches of the river basin, highlighting the need for more sustainable land management policy and water resource management strategies in the future. For example, the large-scale reforestation practices implemented in the study area since 2001 may be problematic given the high water consumption of forests.

Our results show that MC2 performed reasonably in the mountainous UHRB (Fig. 2), which may provide a valuable starting point for other applications of DGVMs to arid and semiarid mountain ecosystems in Asia and beyond. Our MC2 results for 1960–2010 were generally comparable to the half-degree resolution output from the 15 global terrestrial biosphere models (TBMs) published by the Multiscale Synthesis and Terrestrial Model Intercomparison Project (MsTMIP) (Huntzinger et al. 2018). LAI, NPP, and NEP from MC2 fall well within the range of values in the MsTMIP's ensemble of outputs (Fig. 6). However, NPP and ET estimated by MC2 were significantly higher than the MsTMIP ensemble means: NPP and ET were approximately 1.6 and 1.3 times higher, respectively. These comparisons both corroborate the reasonable calibration of MC2 and highlight the possibility that a regionally calibrated high-resolution simulation may capture ecosystem dynamics of mountainous regions that substantially differ from global applications of vegetation models.

Evidence of a good model calibration, notwithstanding large uncertainties remain in dynamic vegetation simulation of the UHRB. We identify several opportunities to improve

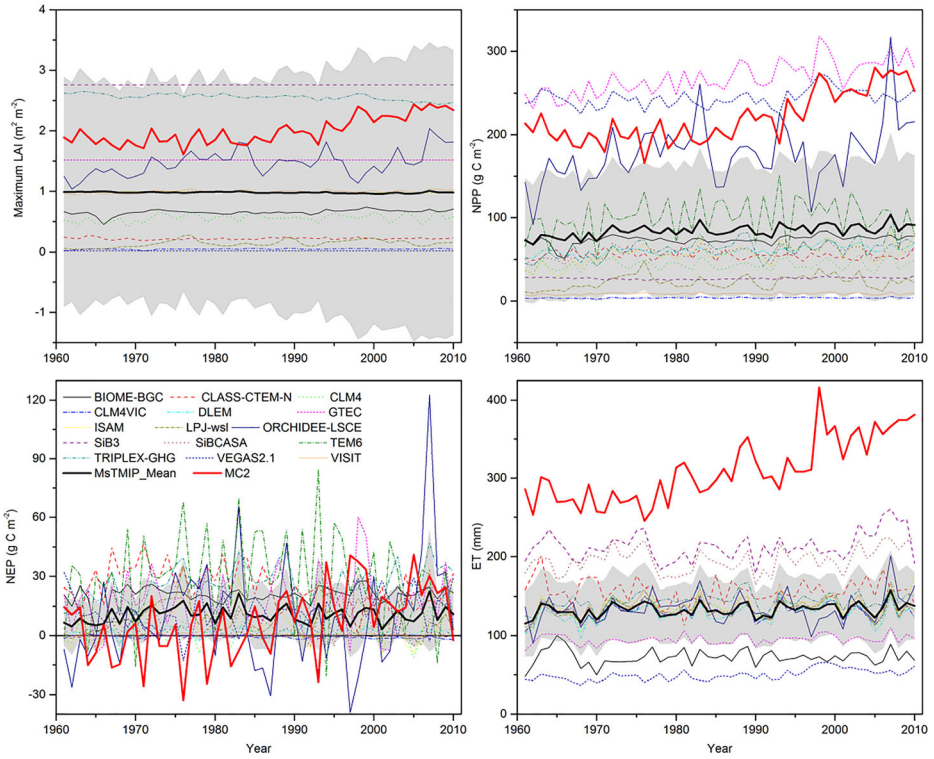

Fig. 6 Maximum leaf area index (**a**), net primary productivity (**b**), net ecosystem productivity (**c**), and evapotranspiration (**d**) simulated by MC2, with corresponding data from the 15 global terrestrial biosphere models (TBMs) published in the Multiscale Synthesis and Terrestrial Model Intercomparison Project (MsTMIP) (Shim et al. 2014). TBM outputs were clipped to the Upper Heihe River Basin. As with MC2, the TBMs are driven by climate, land cover, and atmospheric CO_2 data. BIOME-BGC also simulates the impact of nitrogen deposition. The light gray shaded area represents one standard deviation of the 15 TBM ensemble mean

the input data. First, although the climate data used in this study have been demonstrated to be generally reliable (Ruan et al. 2017), the 1-km spatial resolution may not adequately capture the heterogeneity of microclimates in the UHRB. In particular, slope and aspect may be important factors. Qin et al. (2016b) reported that the vegetation cover, biomass, and SOC on the semi-shady slopes were approximately two times greater than those on the south-facing slopes. Second, we used a future climate projection from a single regional climate model. While the projected warming trend is consistent with warming projected by general circulation models (GCMs), the drying trend projected by the RIEMS 2.0 was contrary to the wetter trend projected by the GCMs (Fig. 1d). In addition to using a single regional climate model, we used only one climate change scenario (RCP4.5). Although RCP4.5 has no probability associated with it (IPCC 2013), using a large ensemble of GCMs with multiple RCPs would more robustly capture the range of possible future changes for the UHRB and quantify the uncertainty arising from GCMs and RCPs. Furthermore, Peterman et al. (2014) found that the MC2 model is very sensitive to soil depth in simulations of carbon and hydrological variables, with correlation coefficients of 0.82. Although the soils data we used were superior to global soil datasets, improved soils data with more samples could alter model outputs, especially in alpine area within the UHRB where only 105 soil profiles were sampled (Yang et al. 2016).

MC2 model structure imposes some limitations. First, MC2 runs on a monthly time step, which may not effectively reflect the effects of weather extremes and freezing/thawing processes on the vegetation shifts and the carbon/water cycles (Beckage et al. 2008; Dolezal et al. 2016; Wipf et al. 2009; Yang et al. 2015). For example, increasing extreme snowfall events in the UHRB (Li et al. 2014) may significantly decrease vegetation cover for both alpine and subalpine communities, with lasting effects (Dolezal et al. 2016). Additionally, warming-induced early snowmelt usually leads to frequent night frosts detrimental to alpine vegetation (Beckage et al. 2008; Dolezal et al. 2016). Second, there are many potentially important ecological processes not simulated by MC2, such as disease, insect outbreaks, invasive species, survival and dispersal capabilities of species, and evolutionary adaptation (Sheehan et al. 2015). Third, our simulations did not directly simulate anthropogenic disturbance, which may partly account for the difference between model output and observation data.

5 Conclusions

Our simulation results show that climate change may have driven substantial shifts in vegetation distribution in the UHRB in the recent past, and characterizes future shifts under the RCP4.5 climate change scenario. The cold barren vegetation type, covering over one-third of the land area in the 1960s, is projected to nearly disappear by the 2070s. Concurrently, ecosystem structure and function are projected to be greatly altered by climate change. The UHRB is simulated to have experienced increases in leaf area index, vegetation productivity, heterotrophic respiration, and evapotranspiration from1961–2010, and those trends are projected to continue into the future, albeit at lower rates. Notably, MC2 simulates a decrease in watershed streamflow since the mid-1980s, and after a period of rapid increase in the near future, the model projects a continued decrease into the future, suggesting possibly severe water shortages in the middle-lower reaches of the watershed. Additionally, MC2 simulates large spatial variability of the vegetation dynamics in response to climate change. These results provide important insights to local land/water management strategies and other applications of DGVMs to mountainous regions. Future studies should continue to improve the input data and model structure to more robustly quantify the potential ecosystem dynamics.

Acknowledgments We thank the Cold and Arid Regions Science Data Center for sharing the climate and vegetation data. We acknowledge the World Climate Research Programme's Working Group on Coupled Modeling, which is responsible for CMIP, and we thank the climate modeling groups (listed in Fig. 1 of this paper) for producing and making available their model output.

Funding information This research was funded by the Natural Science Foundation of China (Grant No. 91425301, 41571026, and 41601196) and the Qinglan Project of Jiangsu Province of China. Partial support was provided by the Southern Research Station of the US Department of Agriculture Forest Service.

References

Bachelet D, Lenihan JM, Daly C, Neilson RP, Ojima DS, Parton WJ (2001) MC1: a dynamic vegetation model for estimating the distribution of vegetation and associated carbon, nutrients, and water—technical documentation. Version 1.0. Gen. Tech. Rep. PNW-GTR-508. U.S. Department of Agriculture, Forest Service, Pacific northwest Research Station, Portland, OR

Bachelet D et al. (2003) Simulating past and future dynamics of natural ecosystems in the United States. Glob Biogeochem Cycles 17

Bachelet D, Ferschweiler K, Sheehan TJ, Sleeter BM, Zhu Z (2015) Projected carbon stocks in the conterminous USA with land use and variable fire regimes. Glob Chang Biol 21:4548–4560

Beckage B, Osborne B, Gavin DG, Pucko C, Siccama T, Perkins T (2008) A rapid upward shift of a forest ecotone during 40 years of warming in the Green Mountains of Vermont. Proc Natl Acad Sci 105:4197–4202

Beniston M (2003) Climatic change in mountain regions: a review of possible impacts. Clim Chang 59:5–31

Case MJ et al. (2018) Climate change, vegetation, and disturbance in South Central Oregon. In: Halofsky JE, Peterson DL, Ho JJ (eds) Climate change vulnerability and adaptation in South Central Oregon. USDA Forest Service, Pacific Northwest Research Station, Portland, OR. (In Press), General Technical Report PNW-GTR-xxxx,

Cheng G, Li X, Zhao W, Xu Z, Feng Q, Xiao S, Xiao H (2014) Integrated study of the water–ecosystem–economy in the Heihe River Basin. Natl Sci Rev 1:413–428

Conklin DR, Lenihan JM, Bachelet D, Neilson RP, Kim JB (2016) MCFire model technical description. Gen. Tech. Rep. PNW-GTR-926. U.S. Department of Agriculture, Forest Service, Pacific northwest Research Station, Portland, OR

Cramer W et al (2001) Global response of terrestrial ecosystem structure and function to CO2 and climate change: results from six dynamic global vegetation models. Glob Chang Biol 7:357–373

Dolezal J et al (2016) Vegetation dynamics at the upper elevational limit of vascular plants in Himalaya. Sci Rep 6:24881

Drapek RJ, Kim JB, Neilson RP (2015) Continent-wide simulations of a dynamic global vegetation model over the United States and Canada under nine AR4 future scenarios. In: Bachelet D, Turner D (eds) Global Vegetation Dynamics. Geophysical Monograph Series. doi:https://doi.org/10.1002/9781119011705.ch6

Gao B, Qin Y, Wang Y, Yang D, Zheng Y (2016) Modeling ecohydrological processes and spatial patterns in the Upper Heihe Basin in China forests 7:10

Gobiet A, Kotlarski S, Beniston M, Heinrich G, Rajczak J, Stoffel M (2014) 21st century climate change in the European Alps—a review. Sci Total Environ 493:1138–1151

Gonzalez P, Neilson RP, Lenihan JM, Drapek RJ (2010) Global patterns in the vulnerability of ecosystems to vegetation shifts due to climate change. Glob Ecol Biogeogr 19:755–768

Gottfried M et al (2012) Continent-wide response of mountain vegetation to climate change. Nat Clim Chang 2:111

Hao L et al (2016) Detection of the coupling between vegetation leaf area and climate in a multifunctional watershed, Northwestern China. Remote Sens 8:1032

Hickler T et al (2012) Projecting the future distribution of European potential natural vegetation zones with a generalized, tree species-based dynamic vegetation model. Glob Ecol Biogeogr 21:50–63

Huntzinger D et al. (2018) NACP MsTMIP: global 0.5-degree model outputs in standard format, version 1.0. ORNL Distributed Active Archive Center

IPCC (2013) *Intergovernmental Panel on Climate Change*. Climate Change 2013: The physical science basis. Contribution of Working Group I to the Fifth Assessment Report of the Intergovernmental Panel on Climate Change. Cambridge Univ. Press, Cambridge, UK and New York, N. Y

Jin H, Li A, Bian J, Nan X, Zhao W, Zhang Z, Yin G (2017) Intercomparison and validation of MODIS and GLASS leaf area index (LAI) products over mountain areas: a case study in southwestern China. Int J Appl Earth Obs Geoinf 55:52–67

Kim JB et al (2017) Assessing climate change impacts, benefits of mitigation, and uncertainties on major global forest regions under multiple socioeconomic and emissions scenarios. Environ Res Lett 12:045001

Kim JB, Kerns BK, Drapek RJ, Pitts GS, Halofsky JE (2018) Simulating vegetation response to climate change in the Blue Mountains with MC2 dynamic global vegetation model. Clim Serv 10:20–32

Lenihan JM, Daly C, Bachelet D, Neilson RP (1998) Simulating broad-scale fire severity in a dynamic global vegetation model. Northwest Sci 72:92–103

Li Z, Li C, Xu Z, Zhou X (2014) Frequency analysis of precipitation extremes in Heihe River basin based on generalized Pareto distribution. Stoch Env Res Risk A 28:1709–1721

Liu P, Hao L, Pan C, Zhou D, Liu Y, Sun G (2017) Combined effects of climate and land management on watershed vegetation dynamics in an arid environment. Sci Total Environ 589:73–88

Liu S et al. (2018) The Heihe integrated observatory network: a basin-scale land surface processes observatory in China Vadose Zone J 17

Luo Y, Wan S, Hui D, Wallace LL (2001) Acclimatization of soil respiration to warming in a tall grass prairie. Nature 413:622–625

Meinshausen M et al (2011) The RCP greenhouse gas concentrations and their extensions from 1765 to 2300. Clim Chang 109:213

Mu C et al (2014) Stable carbon isotopes as indicators for permafrost carbon vulnerability in upper reach of Heihe River basin, northwestern China. Quat Int 321:71–77

Neilson RP (1995) A model for predicting continental-scale vegetation distribution and water balance. Ecol Appl 5:362–385
Nemani RR et al (2003) Climate-driven increases in global terrestrial net primary production from 1982 to 1999. Science 300:1560–1563
Palomo I (2017) Climate change impacts on ecosystem services in high mountain areas: a literature review. Mt Res Dev 37:179–187
Parton WJ et al (1993) Observations and modeling of biomass and soil organic matter dynamics for the grassland biome worldwide. Glob Biogeochem Cycles 7:785–809
Peterman W, Bachelet D, Ferschweiler K, Sheehan T (2014) Soil depth affects simulated carbon and water in the MC2 dynamic global vegetation model. Ecol Model 294:84–93
Piao S, Fang J, Ciais P, Peylin P, Huang Y, Sitch S, Wang T (2009) The carbon balance of terrestrial ecosystems in China. Nature 458:1009
Qin D, Ding Y, Mu M (2016a) Climate and environmental change in China: 1951–2012. Springer, Berlin Heidelberg
Qin Y, Qi F, Holden NM, Cao J (2016b) Variation in soil organic carbon by slope aspect in the middle of the Qilian Mountains in the upper Heihe River Basin, China. Catena 147:308–314
Ruan H et al (2017) Runoff simulation by SWAT model using high-resolution gridded precipitation in the Upper Heihe River Basin, Northeastern Tibetan Plateau. Water 9:866
Running SW, Zhao M (2015) Daily GPP and annual NPP (MOD17A2/A3) products NASA Earth Observing System MODIS land algorithm MOD17 User's Guide
Sheehan T, Bachelet D, Ferschweiler K (2015) Projected major fire and vegetation changes in the Pacific Northwest of the conterminous United States under selected CMIP5 climate futures. Ecol Model 317:16–29
Shim C et al (2014) Evaluation of MODIS GPP over a complex ecosystem in East Asia: a case study at Gwangneung flux tower in Korea. Adv Space Res 54:2296–2308
Song X-D, Brus DJ, Liu F, Li D-C, Zhao Y-G, Yang J-L, Zhang G-L (2016) Mapping soil organic carbon content by geographically weighted regression: a case study in the Heihe River basin, China. Geoderma 261:11–22
Tachikawa T, Hato M, Kaku M, Iwasaki A Characteristics of ASTER GDEM version 2. In: 2011 IEEE International Geoscience and Remote Sensing Symposium, 24–29 July 2011 2011. pp 3657–3660. doi: https://doi.org/10.1109/IGARSS.2011.6050017
Tao F, Zhang Z (2010) Dynamic responses of terrestrial ecosystems structure and function to climate change in China. J Geophys Res Biogeosci 115
Theurillat J-P, Guisan A (2001) Potential impact of climate change on vegetation in the European Alps: a review. Clim Chang 50:77–109
Wang Y, Yang H, Yang D, Qin Y, Gao B, Cong Z (2016) Spatial interpolation of daily precipitation in a high mountainous watershed based on gauge observations and a regional climate model simulation. J Hydrometeorol 18:845–862
Wei Y et al. (2014) NACP MsTMIP: global and North American driver data for multi-model intercomparison. Data set. Available on-line [http://daac.ornl.gov] from oak Ridge National Laboratory Distributed Active Archive Center, Oak Ridge, Tennessee, USA. https://doi.org/10.3334/ORNLDAAC/1220
Wipf S, Stoeckli V, Bebi P (2009) Winter climate change in alpine tundra: plant responses to changes in snow depth and snowmelt timing. Clim Chang 94:105–121
Woodward BFI (1987) Climate and plant distribution. Cambridge University Pre
Wu B, Zhu W, Yan N, Feng X, Xing Q, Zhuang Q (2016) An improved method for deriving daily evapotranspiration estimates from satellite estimates on cloud-free days. IEEE J Selected Topics Appl Earth Obs Remote Sens 9:1323–1330
Xiao Z, Liang S, Wang J, Xiang Y, Zhao X, Song J (2016) Long-time-series global land surface satellite leaf area index product derived From MODIS and AVHRR surface reflectance. IEEE Trans Geosci Remote Sens 54: 5301–5318
Xiong Z, Yan X (2013) Building a high-resolution regional climate model for the Heihe River Basin and simulating precipitation over this region. Chin Sci Bull 58:4670–4678
Yang DW, Bing G, Yang J, Lei HM, Zhang YL, Yang HB, Cong ZT (2015) A distributed scheme developed for eco-hydrological modeling in the upper Heihe River. Sci China Earth Sci 58:36–45
Yang R-M et al (2016) Comparison of boosted regression tree and random forest models for mapping topsoil organic carbon concentration in an alpine ecosystem. Ecol Indic 60:870–878
Yang L, Feng Q, Yin Z, Wen X, Si J, Li C, Deo RC (2017) Identifying separate impacts of climate and land use/cover change on hydrological processes in upper stream of Heihe River, Northwest China. Hydrolog Process 31:1100–1112
You N, Meng J, Zhu L (2018) Sensitivity and resilience of ecosystems to climate variability in the semi-arid to hyper-arid areas of Northern China: a case study in the Heihe River Basin. Ecol Res 33:161–174

Zhang A, Zheng C, Wang S, Yao Y (2015) Analysis of streamflow variations in the Heihe River Basin, northwest China: trends, abrupt changes, driving factors and ecological influences. J Hydrol Reg Stud 3:106–124

Zhang X, Zhou J, Zheng Y (2016) Vegetation map of the Upper Heihe Basin V2.0 Heihe Plan Science Data Center, Lanzhou, China

Zhao Y, Rong Z, Zhang Y, Ye M, Jiang H, Zhao C (2017) Analysis of change in grassland area in the Heihe River basin over the past 30 years and prediction. Acta Pratacul Sin 26:1–15

Zhou D, Zhao S, Liu S, Zhang L (2014) Modeling the effects of the Sloping Land Conversion Program on terrestrial ecosystem carbon dynamics in the Loess Plateau: a case study with Ansai County, Shaanxi province, China. Ecol Model 288:47–54

Affiliations

Decheng Zhou[1] · Lu Hao[1] · John B. Kim[2] · Peilong Liu[1] · Cen Pan[1] · Yongqiang Liu[3] · Ge Sun[4]

[1] Joint International Research Laboratory of Climate and Environment Change (ILCEC)/Jiangsu Key Laboratory of Agricultural Meteorology, Nanjing University of Information Science and Technology, Nanjing 210044, China

[2] Pacific Northwest Research Station, USDA Forest Service, Corvallis, OR 97331, USA

[3] Centers for Forest Disturbance Science, Southern Research Station, USDA Forest Service, Athens, GA 30602, USA

[4] Eastern Forest Environmental Threat Assessment Center, Southern Research Station, USDA Forest Service, Research Triangle Park, NC 27709, USA